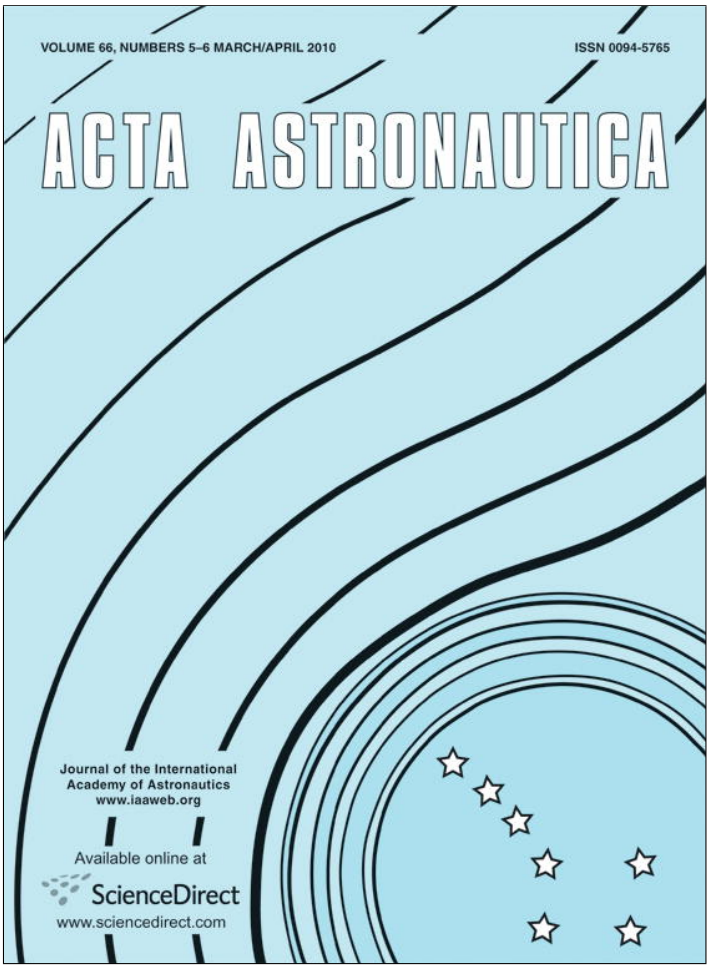

Acta Astronautica 66 (2010) 760–768

Contents lists available at ScienceDirect

Acta Astronautica

journal homepage: www.elsevier.com/locate/actaastro

Transparent heater for study of the boiling crisis near the vapor–liquid critical point

Yves Garrabos [a,*], Carole Lecoutre [a], Daniel Beysens [b,c], Vadim Nikolayev [b,c], Sebastien Barde [d], Gabriel Pont [d], Bernard Zappoli [d]

[a] ESEME-CNRS, Université de Bordeaux, ICMCB UPR9048—87 avenue du Docteur Schweitzer, F 33608 PESSAC Cedex, France
[b] ESEME-PMMH-ESPCI-UMR 7636 CNRS, Universités Paris 6 et Paris 7, 10 rue Vauquelin, F 75231 PARIS Cedex 05, France
[c] ESEME-CEA, 17 rue des Martyrs, F 38054 Grenoble Cedex 09, France
[d] CNES, 18 Avenue E. Belin, F 31401 TOULOUSE Cedex, France

ARTICLE INFO

Article history:
Received 3 February 2009
Accepted 20 August 2009
Available online 22 September 2009

Keywords:
Boiling crisis
Critical heat flux
Liquid–gas critical point

ABSTRACT

New design for a pressurized optical cell dedicated to study the boiling crisis in non-homogeneous critical fluids in microgravity conditions is presented. The main characteristic concerns in situ integration of a heating device as a form of transparent resistive thin layer appropriate for light transmission observation of the liquid film boiling, by monitoring the thermal power produced by this heater. High-resolution and high-speed optical diagnostics complement in situ temperature measurements. Illustrations of the high-level performances are provided by the preliminary results obtained during the Earth's tests of the CNES-DECLIC facility, using two (vertical and horizontal) configurations of the heating device with respect to the gravity field acceleration.

1. Introduction

One of the most efficient ways to transfer heat from solid to gas is boiling phenomena in heated liquid in contact with a solid heater. Such a heating process attracts strong attention from engineers, especially when boiling crisis occurs. Boiling crisis is a transition from a regime where vapor bubbles nucleate separately on the heater wall to a regime where the heater wall is entirely covered by a continuous vapor film. When formed, the vapor film reduces drastically the heat transfer at the heater wall, because of the low gas thermal conduction. The boiling crisis can then produce irremediable damage of the exchanger by melting of the solid heater. This transition phenomenon appears when the heat flux exceeds a threshold value, called the critical heat flux and denoted CHF in the following. The estimation of CHF is essential in the industrial heat exchanger design and management.

In a two-phase critical fluid, a bubble spreading over the heater surface was initially observed [1] while crossing the critical point to reach the homogeneous domain, thanks to the microgravity conditions offered by the Russian MIR station. We have then proposed to investigate by experimental observation while approaching the gas–liquid critical point if the recoil force mechanism can be relevant to give a better understanding of the triggering mechanism at the origin of the boiling crisis. Indeed, we have successively shown by modeling and numerical simulation [2,3] that the thrust of production of vapor can support this gas spreading. This recoil force mechanism was also evidenced by the analysis of the results of a preliminary ground-based experiment where gravity magnetic compensation was produced in a small

* Corresponding author. Tel.: +33 5 40 00 63 37; fax: +33 5 40 00 27 61.
E-mail addresses: garrabos@icmcb-bordeaux.cnrs.fr (Y. Garrabos), lecoutre@icmcb-bordeaux.cnrs.fr (C. Lecoutre), daniel.beysens@espci.fr (D. Beysens), vadim.nikolayev@espci.fr (V. Nikolayev), sebastien.barde@cnes.fr (S. Barde), gabriel.pont@cnes.fr (G. Pont), bernard.zappoli@cnes.fr (B. Zappoli).

0094-5765/$ - see front matter © 2009 Elsevier Ltd. All rights reserved.
doi:10.1016/j.actaastro.2009.08.018

volume of para-hydrogen near its critical point. With remaining steady gravity forces of order $0.02g_0$ (where g_0 is the constant acceleration on Earth's), this last experiment have confirmed that the microgravity conditions which cancel buoyancy forces and generate three-dimensional spheroidal shape of the gas bubble are irreplaceable powerful tools for studying the heat transfer near the gas–liquid–solid contact line.

Our microgravity experimental program to investigate the boiling crisis was planned for the CNES-DECLIC facility [4] that will be used on board the International Space Station (ISS). For that purpose, we have developed new optical pressurized cells designed for future experimental observations of the boiling crisis at low heat fluxes, very close to the CHF. In particular, a new pressurized optical cell integrates an in situ device as a form of a transparent resistive layer ($\sim$50 mm^2 area), appropriate for light transmission observation of the boiling in liquid films.

High-resolution (1000×1000 pixels) and high-speed (462 fr/s) optical diagnostics are synchronized with in situ temperature measurements, and adjusted to the selected monitoring rate of the thermal stimuli produced by the transparent resistive heater. This optical cell is implemented in the Alice-like insert (ALI) of the CNES-DECLIC facility [4,5], which allows the injection of a thermal power 0–3.4 mW and simultaneous data acquisition at high frequency (2 kHz) from 3 thermistors (THERMOMETRICS B10) located inside the fluid. The heat power per unit area can then be controlled in the range 17 mW/m^2–68 W/m^2. Heating period can be adjusted, with a minimum of 43 ms. Resolution from the B10 sensors is better than 0.02 Ω, corresponding to a temperature accuracy around 0.1 mK. In the unexplored range of low heat fluxes, we will expect simplified analysis of the boiling observations, thanks to the low temperature gradients and critical phenomena universality [6] near the critical point of sulfur hexafluoride, using the high capabilities of the CNES-DECLIC instrument [5].

The paper is organized as follows. Section 2 presents the new design for the pressurized optical cell (called DOC for direct observation cell) dedicated to study the boiling crisis in non-homogeneous critical fluids, during the first increment planned for DECLIC utilization on board the Japanese module of ISS. Sections 3 and 4 show some results obtained during preliminary tests performed on Earth's with both the engineering and the flight models of the ALI Inserts, using the heating device either in vertical (Section 3) or horizontal (Section 4) position.

2. Direct observation cell (DOC)

Pictures of the flight model (FM) and engineering model (EM) of the optical cells observed by light transmission are given in (a, b) and (c, d) parts of Fig. 1, respectively. Each fluid sample volume corresponds to a cylindrical volume of $D = 10.6$ mm inner diameter and respective inner thickness $e = 4.115$ mm for the FM cell and $e = 2.637$ mm for the EM cell. Such a fluid sample configuration being observed mainly by wide field light transmission, the cell is called "Direct Observation Cell" (DOC). Moreover, the direct observation cell also allows to record the light scattered at small angles and at 90°. The cells are filled by SF_6 of electronic quality, corresponding to a 99.98% purity (from Air Liquide). The critical coordinates (temperature, pressure, density) of the gas–liquid critical point of SF_6 are $T_c = 318.737$ K (45.587 °C), $p_c = 3.73$ MPa and $\rho_c = 742.6$ kg m^{-3}. The total fluid volume of the FM-DOC is 0.463 cm^3 (including a dead volume mainly due to filling holes), corresponding to a total SF_6 mass of 0.353 g, leading to the filling mean density $\rho = \rho_c + 1.1\%$. For the EM-DOC, the total fluid volume is 0.343 cm^3, the total SF_6 mass is 0.2645 g, and the filling mean density is $\rho = \rho_c + 3.7\%$. The off-critical relative density ρ/ρ_c of each cell was estimated on Earth using a very precise optical method [7] based on the relative variation of the position of the liquid–gas meniscus, as a function of $T - T_c$. On the Earth pictures of Fig. 1, the flat horizontal liquid–gas meniscus at $T_{\mathrm{Lab}} \simeq 298\,\mathrm{K} < T_c$ can be observed around the median position of each cylindrical fluid volume.

Three small (250 μm bead diameter) thermistors (THERMOMETRICS B10, 10 kΩ resistance at 25 °C) are located inside the fluid volume and labeled R5, R6 and R7, respectively. Their positions, clearly visible on the pictures of Fig. 1, are such as we expect to measure three local temperatures close to the gas–liquid interface in microgravity environment (see the discussion below and Fig. 2). The cells were housed in their respective models of the Sample Cell Unit (SCU) and Alice-like Insert (ALI). The SCU temperature is monitored by a very accurate thermal regulation of the DECLIC facility, allowing 10 μK of

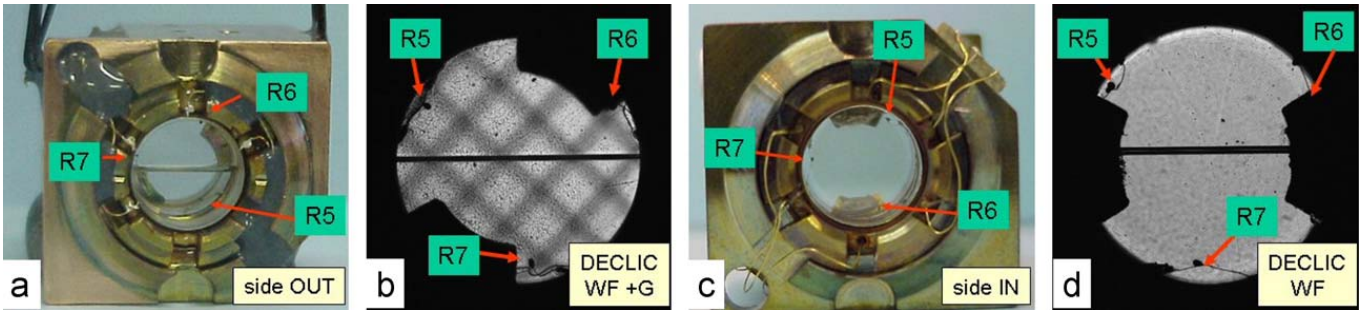

Fig. 1. Earth pictures of the flight model (a, b and of the engineering model (c, d) of the direct observation cells (DOC). (a) and (c) Pictures of the DOC cells before their integration in the Sample Cell Unit of their respective flight and engineering models of Alice-like inserts (ALI) for the DECLIC-CNES facility. (b) Wide field with grid shadowscopy image and (d) Wide field image of these fluid samples, while integrated in their respective ALI insert.

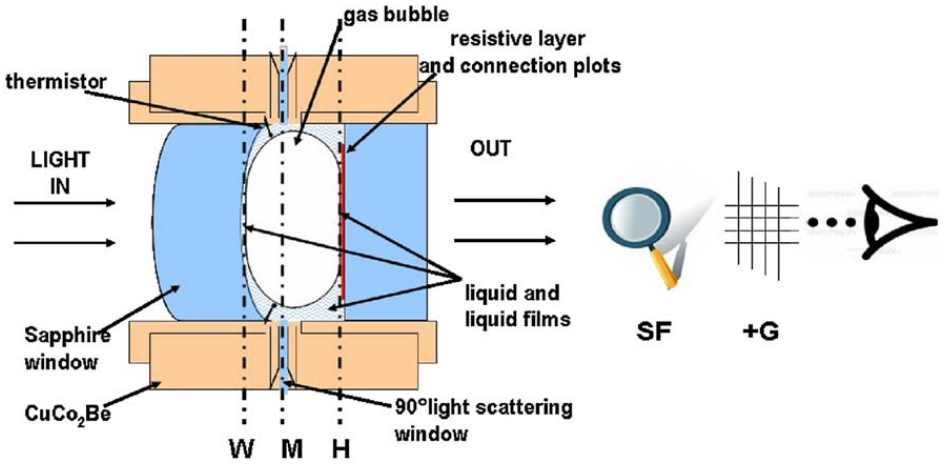

Fig. 2. Schematic cross section (not to scale) of the expected microgravity gas–liquid distribution in the Direct Observation Cell (DOC) dedicated to study the liquid film drying due to the boiling phenomena, using a transparent resistive layer (R8) as a flat local heating source.

relative temperature accuracy for the SCU temperature measurement and $40\,\mu K\,h^{-1}$ of temporal stability, in the range $30-60\,^{\circ}C$. The sensors used for monitoring (label SCUr) and measurements (label SCUm) of the SCU temperature are made of high-stabilized platinum resistors ($100\,\Omega$ resistance at $25\,^{\circ}C$). For additional details concerning the DECLIC facility see Ref. [5].

In the following we describe the specificities of the pressurized optical cell design in regards to the study of the boiling phenomena close to the liquid–gas critical point of SF_6. This cell design (not to scale) is schematized in Fig. 2, where the expected configuration of the gas–liquid phase distribution in microgravity conditions is represented as a central gas bubble surrounded by the liquid wetting the cell walls and sapphire windows. As enlightened by this schematic cross section of the observation path, the two main characteristics of the cell design are the following:

(i) The spherical surfaces of the entrance sapphire window should stabilize the centro-symmetrical $0-g$ configuration of the gas–liquid equilibrium. Indeed, in the expected ideal equilibrium configuration between two equal volumes of coexisting gas and liquid phases in a cylinder of small thickness ($e<D/2$), filled at critical density, the gas bubble is slightly compressed in between the respective inner surfaces of the two opposite sapphire windows. The curved inner surface of the entrance sapphire window acts to symmetrize the compression around the (optical) axis of the fluid cylinder in order to maintain the gas bubble in the same (optical) axial position than the one given by the spheroidal curvature ($R_S \simeq 0.3\,m$, typically) of the entrance window. Such a window design should then prevent any gas bubble displacement which can result from the unavoidable small tilt angle between the inner flat surfaces of two plate windows, or from the highly probable non-central position of the fluid volume in the relative acceleration referential of the orbiter.

(ii) The in situ integration of a thin heating device in the form of a transparent resistive layer (R8), deposited on the inner flat surface of the exit sapphire window. This resistive layer is made from a Sn alloy oxide [8], 8 mm diameter and 200 nm (FM case) or 800 nm (EM case) thickness. The value of its resistance (106 and $46\,\Omega$ in the FM and the EM cases, respectively) is temperature independent ($dR/dT \leq 7\,m\Omega\,K^{-1}$) in the temperature range of present interest. For the two-phase equilibrium state of Fig. 2, we do not expect to observe a direct contact between the gas and the resistive flat layer. Indeed the bubble is separated from the solid inner surface by a thin film of liquid-like mean density, due to the total wetting condition only satisfied for the liquid phase. This particular phase distribution is clearly illustrated in Fig. 2, not to scale since the thin liquid film surrounding the upper gas volume has an estimated thickness of the order of or slightly lower than 100 nm close to the critical point.

The heater resistance, covering a typical area of $50\,mm^2$, is supplied at constant adjustable voltage using two gold plate layers which induce two non-transparent regions in the fluid volume (see, for example, the corresponding black areas in pictures (b) and (d) of Fig. 1 (see also below the different video images of the DOC provided by the DECLIC-CNES facility). The ALI-insert allows injecting an electrical power covering the typical range 0–3.4 mW (ALI-FM) or 0–3.08 mW (ALI-EM), of 12-bits resolution. The heat power per unit area which is dissipated by Joule effect can then be controlled in the range $17\,mW\,m^{-2}$–$68\,W\,m^{-2}$, i.e., a range presently not available in (generally non-transparent) technical devices of same area (and significant larger thickness). We note that this total heat flux (noted q) is split into two parts: one part (noted q_S) is delivered into the solid substrate (i.e., sapphire window) of the resistive layer, while another part (noted q_f) is directly injected in the fluid (with $q = q_S + q_f$ constant). A realistic simplification of the true three-dimensional heat energy dissipation in sapphire and SF_6 considers an infinitely thin constant heat power source q at the ideal thermal interface between these two semi-infinite one-dimensional conductive materials. The corresponding dissipation ratio of $q = cte$ is then

$q_S/q_f = \sigma_S/\sigma_f$ where $\sigma_S = \lambda_S/\sqrt{D_{T,S}} = \sqrt{\lambda_S \rho_S c_{P,S}}$ and $\sigma_f = \lambda_f/\sqrt{D_{T,f}} = \sqrt{\lambda_f \rho_f c_{P,f}}$ are the respective thermal efficiency (i.e., the inverse thermal impedance) of the sapphire and the fluid [$\lambda_i, D_{T,i}, \rho_i$ and $c_{P,i}$ are the respective thermal conductivity, thermal diffusivity, density and specific heat at constant pressure of the sapphire ($i = S$) and SF_6 ($i = f$)]. q_S/q_f is only dependent of the temperature distance to T_c and decreases when $T \to T_c$. That means that less and less thermal energy goes to the substrate approaching T_c, thanks to the increasing thermal efficiency of the critical fluid. Then, the realistic variation of the heat flux dissipated into the fluid $q_f = q/(1 + q_S/q_f)$ can be estimated as a function of $T - T_c$, thanks to the effective heater design and the precise knowledge of the singular thermal properties of SF_6. At $T = T_c + 10$ mK for example, 90% of the electrical power will be dissipated into the fluid.

In addition, the heating period (from a minimum time of 43 ms) can be adjusted (from time increments of 43 ms) in a synchronous manner to the fluid temperature measurements and the digital high resolution (1000× 1000 pixels) or high-speed (up to 462 frame s^{-1}) video recording of the DOC images. These dimensional and shape requirements for the cell design are appropriate for focusing light transmission observation onto the liquid film inserted between the gas bubble and the resistive layer. Especially by using optical microscopy and grid shadowscopy of the DECLIC-CNES instrument [5], we expect to observe and analyze the drying mechanism of the inserted liquid film due to boiling phenomena, monitoring the transparent resistive layer as a local heating source, thanks to the corresponding DECLIC stimuli control [5].

All the high-resolution and high-speed optical diagnostics are synchronized with in situ temperature measurements, and adjusted to the selected monitoring rate of the thermal stimuli produced by the thin resistive transparent layer. The illustrations of the high-level performances of such heating device are provided by the preliminary results obtained during the earth tests using both the engineering model and the flight model of the ALI inserts in the DECLIC-CNES facility. Considering here two characteristic configurations (vertical and horizontal) of the transparent heating device in regards to the earth gravity acceleration, we have reported the experimental observations which satisfy the following main objectives:

(1) To demonstrate the practical efficiency of the transparent heater, either for the single phase fluid cell at $T = T_c + 10$ mK or the two-phase fluid cell at $T = T_c - 10$ mK where the boiling process takes place close to the heating layer;

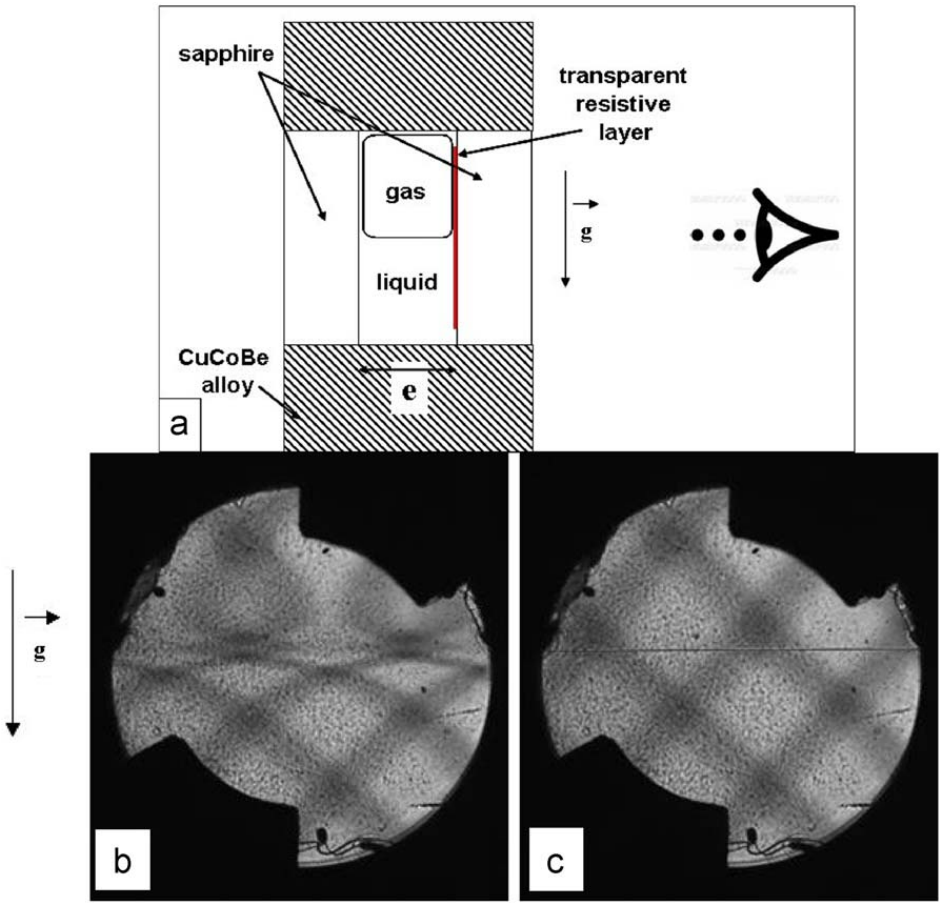

Fig. 3. (a) Schematic illustration of the optical observation setup of the two-phase equilibrium under earth acceleration gravity, directed downwards for the vertical configuration (VC) of the heating device; (b) and (c) high-resolution video pictures of the FM-DOC cell inside DECLIC, observed in transmission using the diagnostic WF + G (see text), before the beginning of the heat pulse, at temperatures +10 and −10 mK relatively to the critical temperature, respectively.

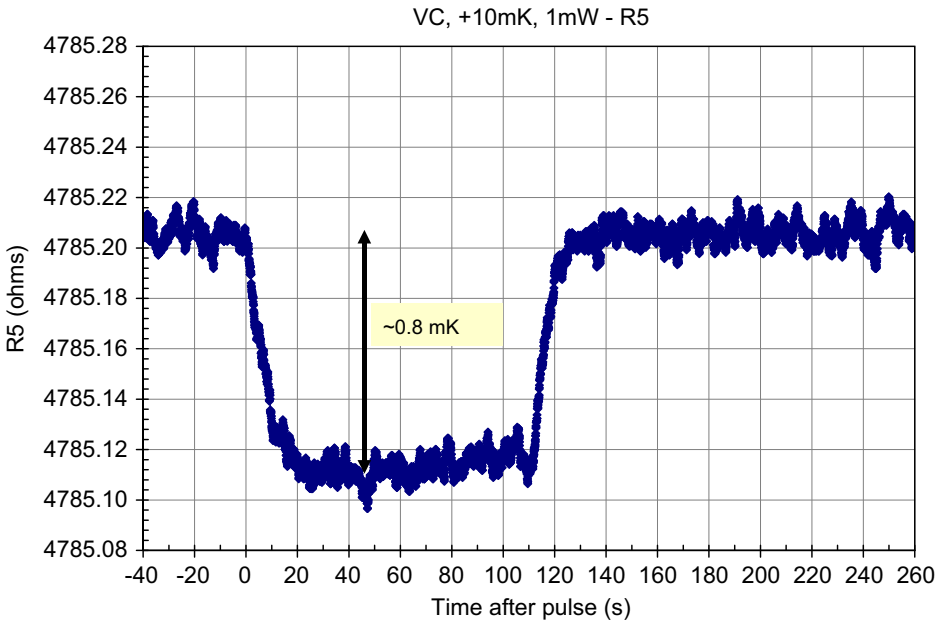

Fig. 4. Measured resistance change for the R5 thermistor during the electrical pulse (1 mW power, 111.3 s duration) in the monophasic regime ($T = T_c + 10$ mK), using the FM-DOC in VC configuration.

(2) To illustrate the specific role of the optical diagnostics in the analysis of the heat and mass transfer inside the fluid sample volume. To simplify the presentation we use WF_p and SF_p for the wide (full) field and the small (microscopy) field imaging of the cell, respectively. The subscript p refers to an object focal plane about the heater ($p = H$), the median ($p = M$) and the entrance window ($p = W$) planes, while the above labels WF_p and SF_p are incremented by $+G$ when the use of the grid shadowscopy diagnostic is added;

(3) To demonstrate the practical importance of the gravity effects near the vapor–liquid critical point, especially using the same low value of the constant heat flux, 18 W m^{-2} typically (i.e., a value which corresponds to the 90% fluid dissipation of a constant electrical power of 1 mW delivered by the transparent resistive layer of 50 mm^2 area). In the following, t_i and t_e are the respective starting and ending time of each selected heat pulse at constant power.

3. Heating in the vertical wall configuration

Fig. 3(a) gives a schematic configuration of the optical cell where the light transmission is made along the horizontal axis of the fluid cylinder while the vertical transparent resistive layer is then parallel to the earth gravity acceleration. We use the label "VC" for this vertical heater configuration which corresponds to the nominal up–down position of the DECLIC instrument on Earth. In the two-phase regime, the film heater is directly wet by the (film and bulk) liquid and can initially act in the gas only through the thin film of liquid-like mean density. This usual phase distribution on earth (see pictures (b) and (d) of Fig. 1) is illustrated (not to scale) in Fig. 3(a). In the two following subsections, we successively discuss the results obtained when performing an electrical pulse (1 mW power; 111.3 s duration), either at $T = T_c + 10$ mK (single-phase regime, see Section 3.1) or at $T = T_c - 10$ mK

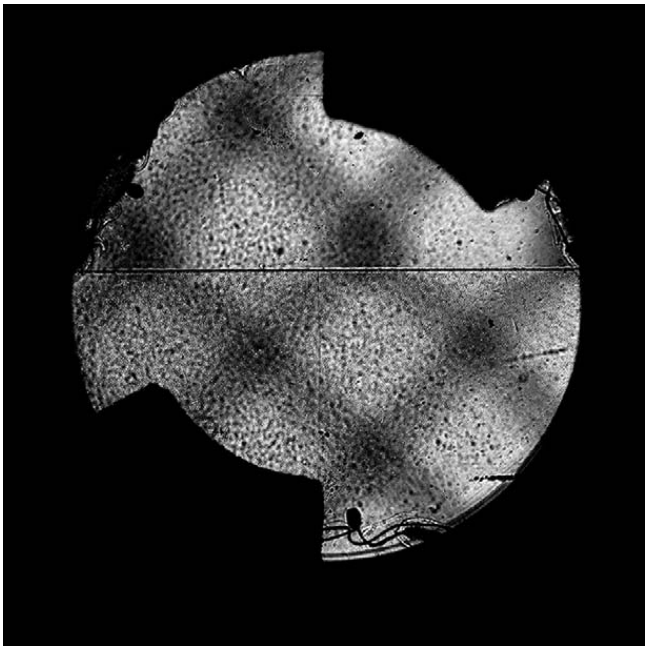

Fig. 5. Wide field transmission added to grid shadowscopy of SF_6 fluid sample, 50 s after the start of an electrical pulse (1 mW power, 111.3 s duration) in the two-phase regime ($T = T_c - 10$ mK), considering VC configuration for the FM-DOC. Gravity is directed downwards. The nucleate boiling close to the transparent heater is observed. A convective vapor channel is visible along the vertical medium axis of the liquid part [see also Fig. 6(c)].

(two-phase regime, see Section 3.2) in the FM-DOC. Figs. 3(b) and (c) show the $WF_H + G$ video pictures of each respective initial equilibrium state of the FM cell, before to perform the corresponding heat pulse. The use of the grid shadowscopy on Fig. 3(b) allows visualization of remaining density gradients inside the fluid cell before the thermal pulse. In the two-phase case which is shown in Fig. 3(c), the position of the liquid–gas meniscus in this VC configuration is visible close to the cell mid-height.

3.1. Heat and mass transfers in the single phase region at $T = T_c + 10\,\mathrm{mK}$

We expected to observe convective flows in the heated fluid boundary layer close to the vertical heater which is a well-known unstable heated fluid configuration with no instability threshold. However, at this temperature distance and for the small value of the heat flux, the flows were hardly visible. Nevertheless, the shadowscopy video pictures have evidenced density evolution during the heat pulse. This is confirmed by the R5 thermistor response reported in Fig. 4 which shows that the (small) convective flow appears and disappears rapidly at the beginning and stoping periods of the heat pulse. In addition, the maximum resistance change of $\simeq 0.1\,\Omega$ corresponds to a very small temperature variation of $\simeq 0.8\,\mathrm{mK}$ (with $dR/dT = 165\,\Omega\,\mathrm{K}^{-1}$ at this experimental fluid temperature). We note that resolution of the temperature measurements from this B10 sensor reaches typically $10\,\mu\mathrm{K}$.

3.2. Heat and mass transfers in the two-phase region at $T = T_c - 10\,\mathrm{mK}$

Fig. 5 shows a $WF_H + G$ video picture of the fluid sample during the thermal heat pulse, at $t_i + 50\,\mathrm{s}$, when focussed on the vertical transparent heater. We observe the nucleate boiling regime in the liquid domain in contact with the transparent heater. Along the vertical medium axis of the liquid part, a vapor channel is formed by convective motion [see also Fig. 6(c)]. Fig. 6(a) gives a SF_H picture, just after the beginning of the heat pulse, where the vapor bubbles nucleate on the transparent heater surface. The vapor bubble convective motions are observed on a SF_H picture of Fig. 6(b), 7.8 s after the

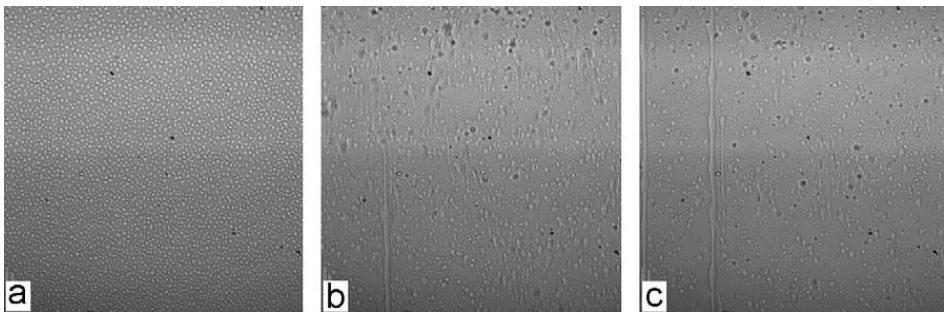

Fig. 6. Small field (SF_H) observations of SF_6 fluid sample focussed on the transparent heater, during the electrical pulse (1 mW power, 111.3 s duration) in the two-phase regime ($T = T_c - 10\,\mathrm{mK}$), using the FM-DOC in VC configuration; (a) 1.3 s, (b) 7.8 s and (c) 50 s after starting of the pulse. Gravity is directed downwards. The initial nucleation of small vapor bubbles on the heater surface is shown in (a), while the bubble convective motions are noticeable in (b). The formation of convective vapor channels close to the heater is visible in picture (c).

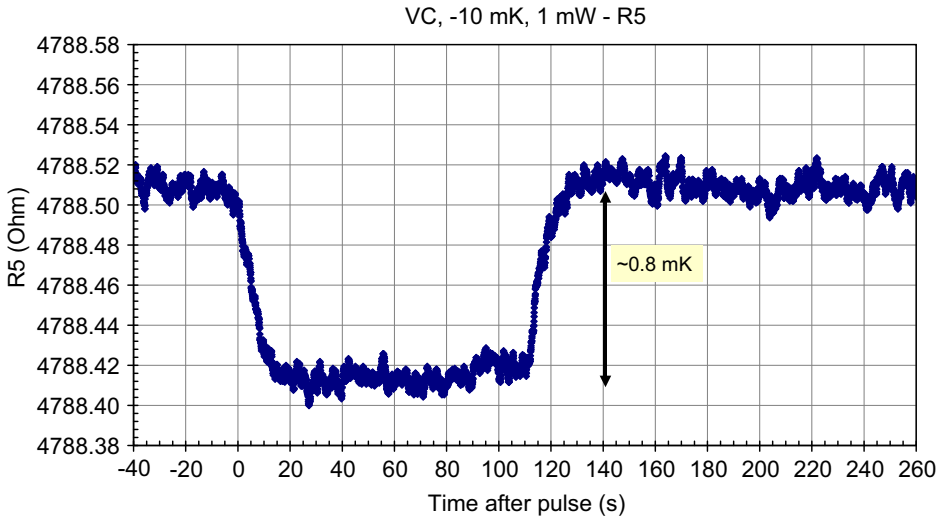

Fig. 7. Measured resistance change for the R5 thermistor during the electrical pulse (1 mW power, 111.3 s duration) in the two-phase region ($T = T_c - 10\,\mathrm{mK}$), using the FM-DOC in VC configuration.

beginning of the heat pulse. The formation of convective vapor channels close to the heater, 50 s after the beginning of the heat pulse, is visible on the SF_H picture of Fig. 6(c).

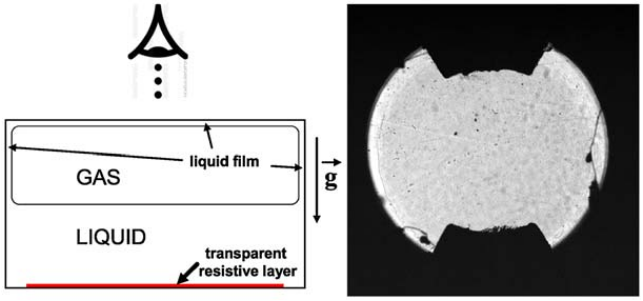

Fig. 8. Schematic illustration (left) of the observation by light transmission of the two-phase equilibrium on earth for the "cooker" configuration (CC) where the heating device is located at the bottom of the DOC cell, and example of a WF_H video picture (right) focussed on the transparent heater for the EM-DOC.

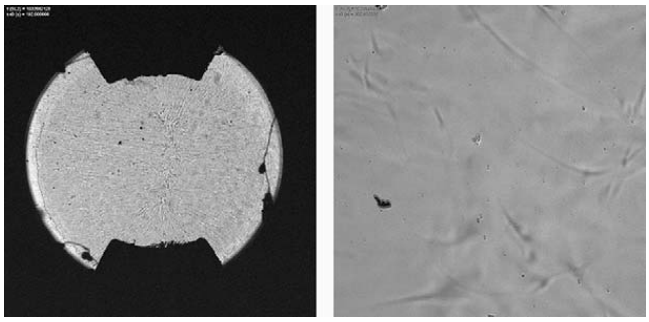

Fig. 9. Video pictures WF_H and SF_H of transmission observation of SF_6 fluid sample in wide field (left) and small field (right), 192 s after the beginning of an electrical pulse (1 mW power, 200 s duration) in the single phase domain ($T = T_c + 10$ mK), using the EM-DOC in CC configuration. Each observation is focused on the heating device, at the bottom of the cell (see text).

In addition, in this VC configuration where the thermistor R5 of the FM-DOC cell is located in the gas domain, the R5 response reported in Fig. 7 confirms the existence of convective flows in the gas phase, quasi-synchronous with the heat pulse duration.

4. Heating in the pressurized "cooker" configuration

Fig. 8 (left) gives the second schematic configuration of the optical cell where the light transmission is made along the vertical axis of the fluid cylinder, while the horizontal transparent resistive layer acts at the bottom of the vertical fluid cylinder. The heating device is then perpendicular to the earth gravity acceleration, only in contact with the liquid part of the two-phase cell configuration. This pressurized "cooker" configuration which is obtained for one specific right angle position of the DECLIC instrument on Earth is labeled "CC" . The optical set up of the top observation of the two-phase distribution on earth is illustrated (not to scale) in Fig. 8 (left). The full view imaging of the cell needs to integrate the light paths in a layered medium.

The following presentation of the heat pulse results uses a similar organization as in Section 3. However, the heat pulses (1 mW power; 200 s duration) are now performed using the EM-DOC cell, at $T = T_c \pm 10$ mK. Fig. 8 (right) shows a video picture of an initial two-phase equilibrium state of the EM-DOC cell for this CC case, just before the heat pulse.

4.1. Heat and mass transfers in the single phase region at $T = T_c + 10$ mK

Fig. 9 shows video pictures, one WF_H (left) and one SF_H (right), respectively, of the cell at the time 192 s after the beginning of the heat pulse, at a temperature around 10 mK above the critical temperature. Convective flows are rapidly observed in this CC configuration, and also stop very rapidly after the end of the pulse. Fig. 10 reports the

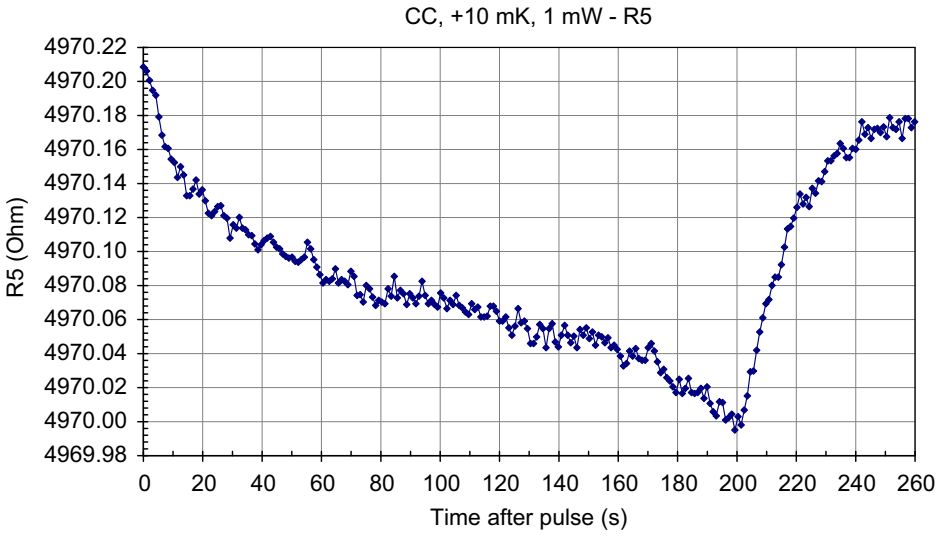

Fig. 10. Measured resistance change of the R5 thermistor sensor during the electrical pulse (1 mW power, 200 s duration) in the monophasic regime ($T = T_c + 10$ mK), using the EM-DOC in CC configuration.

R5 sensor response during the heat pulse where the maximum resistance change of $\simeq 0.2\,\Omega$ corresponds to a local temperature variation of the fluid of $\simeq 1.5$ mK (with $dR/dT \simeq 165\,\Omega\,K^{-1}$ at this experimental fluid temperature).

4.2. Heat and mass transfers in the two-phase region at $T = T_c - 10$ mK

Fig. 11 shows two video pictures WF_H (left) and SF_H (right) of the fluid sample focused on the transparent heater, 50 s after the beginning of the heat pulse, at a temperature about 10 mK below the critical temperature. The picture (a) shows the nucleate boiling regime. We note that this two-phase mechanism is clearly distinguishable by comparison with the one-phase convective motions shown in the similar picture Fig. 9 (right).

Figs. 12(a)–(c) give small field observations of the fluid sample at $t_i + 50$ s, for three different focal planes. Gravity is directed perpendicular to the plane of the images, from the upper sapphire window [SF_W, see picture (c)] toward the bottom transparent heater [SF_H, see picture (a)]. Fig. 12(a) shows the vapor bubble nucleation on the transparent heater surface. Fig. 12(b), which is focussed on the vapor–liquid interface (SF_M), distinguishes the rising vapor bubbles from the falling liquid droplets. When focussed on the curvated inner surface of the upper sapphire window (SF_W), the image of Fig. 12(c) shows the formation of the falling liquid droplets (see also next Fig. 13). The Rayleigh–Taylor-like instability in the liquid wetting film at the top of the cell explains the droplet formation mechanism. From this layered observation of the fluid sample during the thermal heat pulse, we have been able to schematize in Fig. 13 the convective flows of matter in the two-phase fluid cell heated in "cooker" configuration.

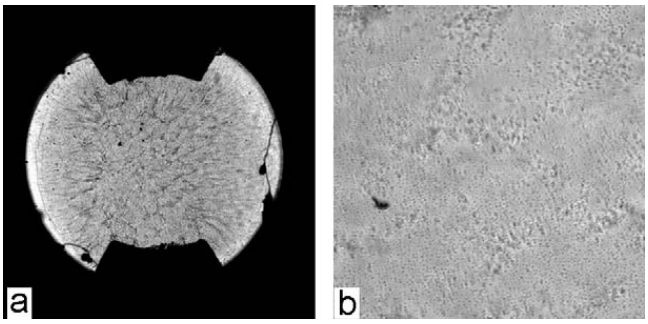

Fig. 11. Video pictures WF_H and SF_H of transmission observation of SF_6 fluid sample in wide field (a) and microscopy (b), during a thermal pulse (1 mW power, 200 s duration) in the two-phase regime ($T = T_c - 10$ mK), using the EM-DOC with CC configuration. Each observation is focussed on the transparent resistive heating layer, at the bottom of the cell. The nucleate boiling regime is visible in (b) and clearly distinguishable by comparison with the similar picture Fig. 9 (right) obtained in the single phase regime.

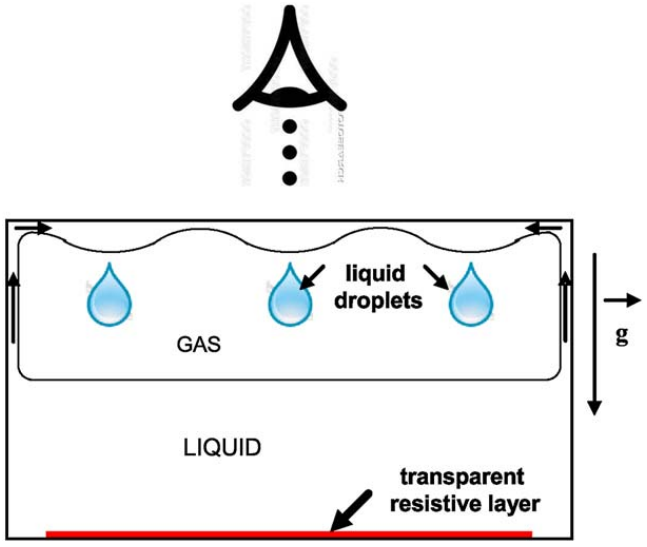

Fig. 13. Schematic illustration of the flows of gas and liquid in the two-phase regime, using the transparent heater device for the pressurized cooker configuration (CC) of the fluid cell on Earth.

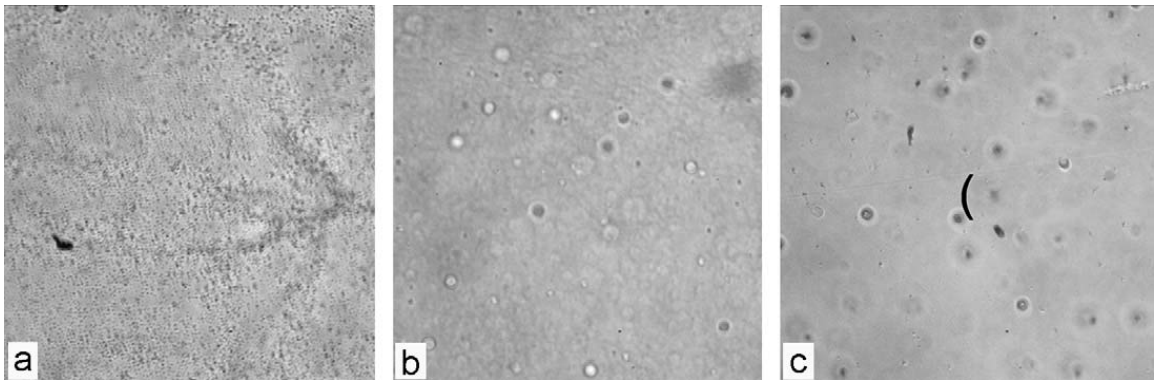

Fig. 12. Small field ($SF_{H,M,W}$) observations of SF_6 fluid sample, 50 s after starting on an electrical pulse (1 mW power, 200 s duration) in the two-phase regime ($T = T_c - 10$ mK), using the EM-DOC in CC configuration; (a) image focused on the transparent heater (SF_H) showing the vapor bubble nucleation; (b) image focused on the vapor–liquid interface (SF_M) showing the (rising) small vapor bubbles and the (falling) liquid droplets; (c) image focused on the curvated inner surface of the upper sapphire window (SF_W) showing the formation of the falling liquid droplets (see text and next Fig. 13). Gravity is directed perpendicular to the plane of the images, from the upper sapphire window (SF_W) toward the bottom transparent heater (SF_H).

5. Conclusion

We have proposed to investigate the triggering mechanism at the origin of the boiling crisis by direct observation of a gas bubble spreading over a transparent heater surface, during the heating of a critical two-phase sample cell filled by SF_6. The main originalities of these new investigations are provided by monitoring of low heat fluxes and control of the liquid–vapor properties, by fine adjustment of the distance to the critical point. Especially using an in situ heating device as a form of transparent resistive layer appropriate for light transmission observation of the liquid films, we have shown the high capabilities of the DECLIC-CNES instrument to analyze the convective flows which are superimposed to the boiling process on Earth's conditions. The microgravity conditions which cancel buoyancy forces and generate three-dimensional spheroidal shape of the gas bubble remain an irreplaceable powerful tool for studying the boiling crisis. The above results obtained during the ground-based tests of the transparent heater are promising for the study of the boiling crisis using the ALI-DECLIC facility on board the International Space Station.

Acknowledgements

The authors acknowledge the financial support from CNES (Centre National d'Etudes Spatiales). They gratefully thank Eric Georgin for his assistance during the cell integration and Jean-Pierre Manaud, Iyad Saadeddin and Guy Campet for development and processing of the thin resistive layer made of Sn alloy oxide. They also thank the CNES-DECLIC project team, especially project manager Gerard Cambon, and the associated DECLIC industrial teams (ASTRIUM-ST, COMAT, EREMS, IDEAS, SODERN, SEIV-Aquitaine, AXS, ARCOFLUID) for their help during the accomplishment of this work.

References

[1] Y. Garrabos, C. Lecoutre-Chabot, J. Hegseth, V. Nikolayev, D. Beysens, J.P. Delville, Phys. Rev. E 64 (2001) 051602.
[2] V. Nikolayev, D. Chatain, Y. Garrabos, D. Beysens, Phys. Rev. Lett. 97 (2006) 184503.
[3] V. Nikolayev, D. Chatain, D. Beysens, Y. Garrabos, Boiling crisis and evaporation at the triple contact line, in: ISPS 2007, 2007.
[4] G. Cambon, B. Zappoli, S. Barde, F. Duclos, R. Lauver, R. Marcout, G. Raymond, D. Beysens, Y. Garrabos, C. Lecoutre, B. Billia, N. Bergeon, N. Mangelinck, in: 55th International Astronautical Congress, Paper IAC-IAF/IAA-04-J.5.03, 2004.
[5] R. Marcout et al., in: Proceedings of the IAC-2006, Valencia, Spain, 2–6 October 2006, IAC-06-A2.5.02; see also 〈http://smsc.cnes.fr/DECLIC/index.htm〉. We note that the second cell of the ALI insert, called Interferometry Observation Cell (IOC), placed in an arm of a Twyman-Green interferometer of the ALI-Insert of the DECLIC instrument [5] is not described here. The expected configuration of the gas–liquid phase distribution in microgravity conditions is there represented as two symmetric gas bubbles surrounded by the liquid wetting the cell walls, the sapphire windows, and the walls of a massive heater. The main characteristic of IOC design concerns in situ integration of a heating device as a form of massive fluxmeter appropriate to interferometry observation of the shape deformation of the vapor liquid interface.
[6] See for example, M.A. Anisimov, J.V. Sengers, in: J.V. Sengers, R.F. Kayser, C.J. Peters, H.J. White, Jr. (Eds.), Equations of State for Fluids and Fluid Mixtures, Part I, Elsevier, Amsterdam, UK, 2000, pp. 381–434.
[7] C. Morteau, M. Salzmann, Y. Garrabos, D. Beysens, in: A. Viviani (Ed.), Proceedings of the Second European Symposium on Fluids in Space, April 22–26, 1996, Naples, Italy, 1996, pp. 327–333.
[8] I. Saadeddin, Ph.D. Thesis, Université Sciences et Technologies - Bordeaux I (30/03/2007), B. Pecquenard; G. Campet (Dir.) [tel-00373315-version 1].